Protein−Carbohydrate Interactions Defining Substrate Specificity in *Bacillus* 1,3-1,4-β-D-Glucan 4-Glucanohydrolases as Dissected by Mutational Analysis[†]

Kirill Piotukh,[‡] Violeta Serra,[§] Rainer Borriss,[‡] and Antoni Planas*[,§]

Laboratory of Biochemistry, Institut Químic de Sarrià, Universitat Ramon Llull, Via Augusta 390, 08017 Barcelona, Spain, and Fachbereich Biologie, Humboldt Universität, Berlin, Federal Republic of Germany

Received July 22, 1999

ABSTRACT: The carbohydrate-binding site of *Bacillus macerans* 1,3-1,4-β-D-glucan 4-glucanohydrolase has been analyzed through a mutational analysis to probe the role of protein−carbohydrate interactions defining substrate specificity. Amino acid residues involved in substrate binding were proposed on the basis of a modeled enzyme−substrate complex [Hahn, M., Keitel, T., and Heinemann, U. (1995) *Eur. J. Biochem. 232*, 849−859]. The effects of the mutations at 15 selected residues on catalysis and binding were determined by steady-state kinetics using a series of chromogenic substrates of different degree of polymerization to assign the individual H-bond and hydrophobic contributions to individual subsites in the binding site cleft. The glucopyranose rings at subsites −III and −II are tightly bound by a number of H-bond interactions to Glu61, Asn24, Tyr92, and Asn180. From k_{cat}/K_M values, single H-bonds account for 1.8−2.2 kcal mol^{-1} transition-state (TS) stabilization, and a charged H-bond contributes up to 3.5 kcal mol^{-1}. Glu61 forms a bidentated H-bond in subsites −III and −II, and provides up to 6.5 kcal mol^{-1} TS stabilization. With a disaccharide substrate that fills subsites −I and −II, activation kinetics were observed for the wild-type and mutant enzymes except for mutations on Glu61, pointing to an important role of the bidentate interaction of Glu61 in two subsites. Whereas removal of the hydroxyl group of Tyr121, initially proposed to hydrogen-bond with the 2OH of Glc*p*-I, has essentially no effect (Y121F mutant), side-chain removal (Y121A mutant) gave a 100-fold reduction in k_{cat}/K_M and a 10-fold lower K_I value with a competitive inhibitor. In subsite −IV, only a stacking interaction with Tyr22 (0.7 kcal mol^{-1} TS stabilization) is observed.

1,3-1,4-β-Glucan is the major polysaccharide of the endosperm cell wall of cereals. It is mainly composed of cellotriosyl and cellotetraosyl units linked through a single β-1,3 glycosidic bond. Enzymatic depolymerization of this polysaccharide is an early event in the germination process, catalyzed by endogenous glycosidases with three different specificities: 1,4-β-glucan 4-glucanohydrolase (EC 3.2.1.4), 1,3-β-glucan 3-glucanohydrolase (EC 3.2.1.39), and 1,3-1,4-β-glucan 4-glucanohydrolase (EC 3.2.1.73). The latter is the most efficient and has a strict specificity for hydrolysis of β-1,4 glycosidic bonds in 3-*O*-substituted glucopyranose units (*1*, *2*).

1,3-1,4-β-Glucan 4-glucanohydrolases (1,3-1,4-β-glucanases)[1] are also found in bacteria. The plant and microbial enzymes have neither sequence similarity nor related three-dimensional structures. Whereas the former belong to family 17 of glycosyl hydrolases (*3*, *4*), the bacterial enzymes are members of family 16. Genes from different *Bacillus* species, *Fibrobacter succinogenes*, *Ruminococcus flavofaciens*, *Clostridium thermocellum* (*5*), *Streptococcus bovis* (*6*), and *Orpinomyces* (*7*) have been cloned and the enzymes characterized. They are monodomain proteins with molecular masses of 25−30 kDa and basic pI (8−9), active in a wide pH range, and quite thermostable compared to the plant enzymes.

A large body of biochemical and structural data has been accumulated recently on the *Bacillus* 1,3-1,4-β-glucanases. They are retaining glycosidases (*8*) acting by general acid−base catalysis in a double-displacement mechanism (*9*, *10*). Mutational analyses on both *B. licheniformis* (*11*) and *B. macerans* (*12*) have identified the essential catalytic residues, Glu103 as the catalytic nucleophile and Glu107 as the general acid/base (*B. macerans* numbering), and their functional roles have been probed by a chemical rescue methodology (*13*).

Synthetic low molecular weight oligosaccharides **1a**−**e** (Scheme 1) (*14*, *15*), together with other series of aryl and methyl glycosides, have been used for kinetic and mechanistic studies of wild-type and mutant *B. licheniformis* enzymes (*16*, *17*, Viladot et al. manuscript in preparation). It has been shown that the binding site cleft is composed of six subsites (four on the nonreducing end from the scissile glycosidic bond, and two on the reducing end), and that the first step of the mechanism leading to the glycosyl−enzyme

[†] This work was supported by Grants BIO97-0511-C02-02 from the Plan Nacional de Biotecnología, CICYT, Spain (to A.P.) and BO 1113/1-3 from the Deutsche Forschungsgemeinschaft DGF, Germany (to R.B.).

* To whom correspondence should be addressed. E-mail: aplan@iqs.url.es.

[‡] Humboldt Universität.

[§] Universitat Ramon Llull.

[1] Abbreviations: 1,3-1,4-β-glucanase, 1,3-1,4-β-D-glucan 4-glucanohydrolase (or lichenase); H(A16M), hybrid 1,3-1,4-β-glucanase (amino acids 1−16 from *Bacillus amyloliquefaciens*, 17−212 from *Bacillus macerans*); TS, transition state.

10.1021/bi991690q CCC: $18.00
Published on Web 11/16/1999

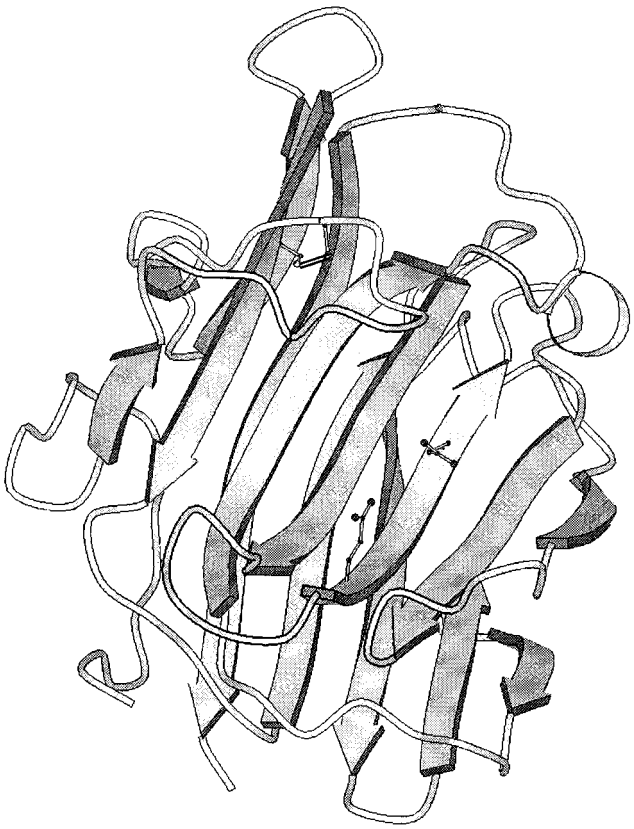

FIGURE 1: 3D-structure of *Bacillus* 1,3-1,4-β-glucanase. The side chains of the catalytic residues E103 and E107 are shown. PDB entries: 1MAC (*B. macerans*), 1GBG (*B. licheniformis*), 2AYH [H(A16M) hybrid], 1BYH [covalent H(A16M)-epoxybutyl cellobioside complex]. Drawn with MOLSCRIPT (*43*).

Scheme 1: Chromophoric Synthetic Substrates **1a**−**e** and Inhibitor **2** Used in This Study

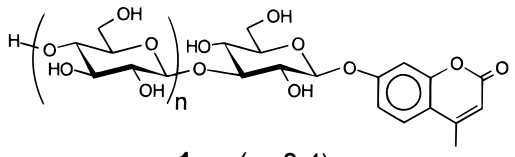

1a-e (n= 0-4)

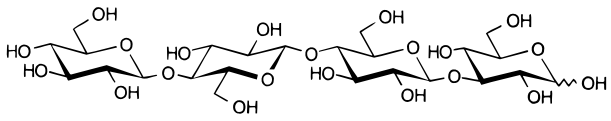

2

intermediate is rate determining for activated aryl glycoside substrates.

The three-dimensional structure of two wild-type *Bacillus* 1,3-1,4-β-glucanases [*B. licheniformis* (*18*) and *B. macerans* (*12*)] and several hybrids (*B. amyloliquefaciens*−*B. macerans*) and circularly permuted proteins (*19*) have been solved by X-ray crystallography. A deep channel runs across the concave side of the 1,3-1,4-β-glucanase jellyroll β-sandwich fold which contains a number of aromatic amino acid residues on its walls and acidic residues at the bottom. This carbohydrate-binding cleft is defined by two structural elements (Figure 1): a loop that partially covers the distant subsites on the nonreducing end from the site of hydrolysis and a large β-sheet on the concave face of the molecule composed of six antiparallel β-strands that shape the entire cleft. Whereas loop residues have been analyzed through an alanine scanning mutagenesis approach (*20*), the overall binding site cleft remains to be studied. The crystal structure of the hybrid H(A16M) with a covalently bound epoxybutyl cellobioside inhibitor has also been solved, with the suicide inhibitor bound to the catalytic nucleophile Glu103 (*21*). This structure, however, is not a good model to analyze protein−carbohydrate interactions because a butyl chain instead of a Glc*p* ring occupies subsite −I, and only a cellobiosyl unit is bound into the cleft.

To understand the structural basis of the strict specificity of bacterial 1,3-1,4-β-glucanases, an extensive mutational study was undertaken aimed at evaluating the individual protein−carbohydrate interactions in the productive enzyme−substrate complex. Since no 3D-structure of a noncovalent enzyme−substrate or enzyme−inhibitor complex is yet available, the current analysis is based on a modeled structure due to Hahn et al. (*22*). A hexasaccharide of structure G4G4G3G4G4G, a true substrate consisting of a barley β-glucan fragment that fills the six subsites of the binding site cleft (−IV to +II), was built into the active-site channel of the free hybrid H(A16M) X-ray structure. After molecular dynamics and energy minimization, all the Glc*p* rings remain in the low-energy $^4C_1$ conformations. The ligand describes a smooth path through the channel, with a deflection at the β-1,4 linkage between subsites −I and +I, where the scissile glycosidic bond is strained. As compared to the structure of the covalent H(A16M)-epoxybutyl cellobioside inhibitor (*21*), the side chains of the residues in the binding-site cleft have essentially the same orientations, except His97 that interacts with the covalently bound inhibitor, but is oriented far from the substrate in the modeled structure. A summary of the observed interactions in the E·S model is presented in Figure 2, and the 3D details are shown in Figures 5 and 6. The proposed interactions are analyzed here for the *Bacillus macerans* 1,3-1,4-β-glucanase by kinetic analysis of single point mutants with a series of chromogenic substrates **1a**−**e**.

MATERIALS AND METHODS

Bacterial Strains and Culture Media. Escherichia coli DH5α [*supE44* Δ*lacU169* (*ϕ80 lacZ*Δ*M15*)*hsdR17 recA1 endA1 gyrA96 thi-1 relA1*] was used for plasmid propagation, transformation with the mutagenic polymerase chain reaction (PCR) products, and protein expression from mutant genes. For plasmid isolation and expression, bacteria were grown in LB medium. Ampicillin at 100 μg/mL was added when appropriate.

Chemicals and Enzymes. Restriction endonucleases and T4 DNA ligase were from New England Biolabs Inc., and Replitherm DNA polymerase was purchased from Epicenter technologies. DNA sequencing was performed with the T7 sequencing kit from Pharmacia Biotech, Oligonucleotides were synthesized by Gibco BRL Custom Primers.

Substrates and Inhibitors. The chromogenic substrates for enzyme kinetics, 4-methylumbelliferyl β-D-glucopyranoside (G-MU, **1a**), 4-methylumbelliferyl 3-*O*-β-D-glucopyranosyl-β-D-glucopyranoside (G3G-MU, **1b**), 4-methylumbelliferyl 3-*O*-β-cellobiosyl-β-D-glucopyranoside (G4G3G-MU, **1c**), 4-methylumbelliferyl 3-*O*-β-cellotriosyl-β-D-glucopyranoside (G4G4G3G-MU, **1e**) and 4-methylumbelliferyl 3-*O*-β-cello-

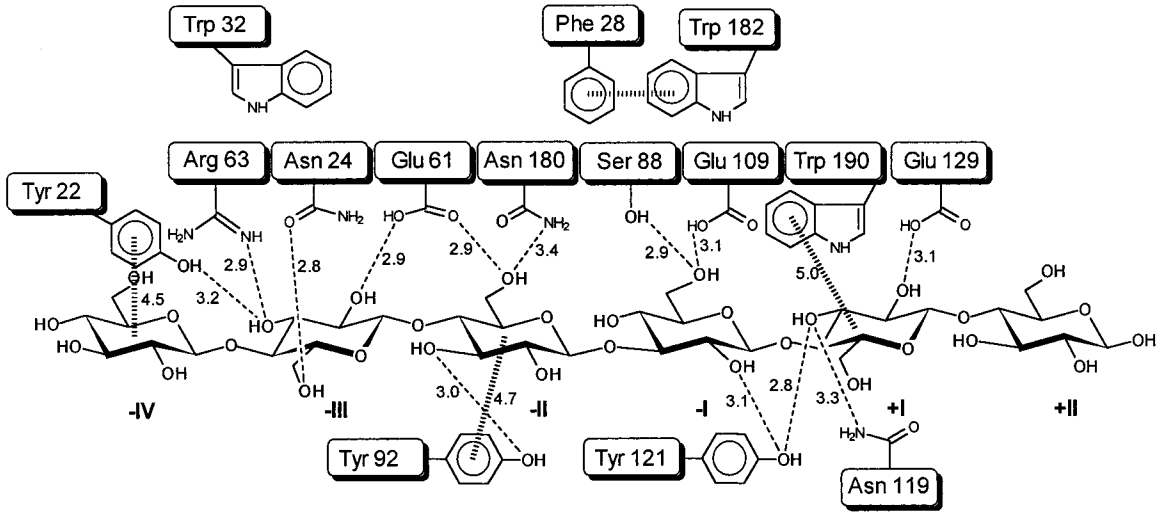

FIGURE 2: Scheme of protein carbohydrate interaction proposed by molecular modeling (*22*). (···) Hydrogen-bonding interactions (distance between heteroatoms in Å), (||||) stacking interactions (distance between center of gravity of the rings in Å).

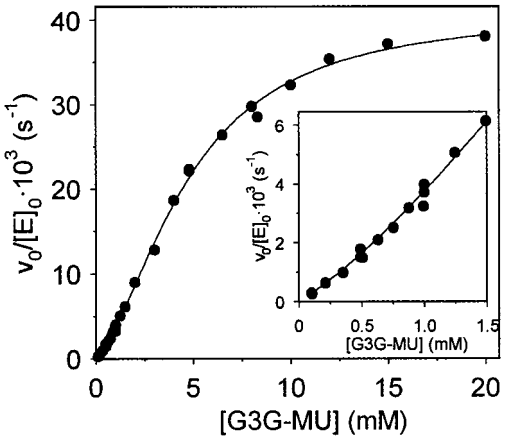

FIGURE 3: Kinetics of the enzyme-catalyzed hydrolysis of substrate **1b** by the wild-type enzyme. Data of $v_0/[E]_0$ vs [S] were fitted to eq 4. (Inset) Magnification at low substrate concentration.

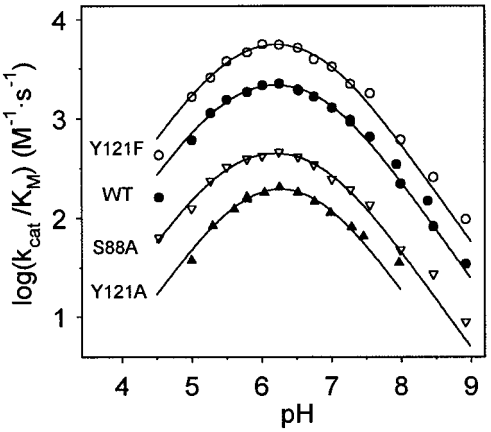

FIGURE 4: pH dependence of k_{cat}/K_M with substrate **1c** for wild-type and subsite −I mutants. Fitted data and experimental conditions are in Table 4.

tetraosyl-β-D-glucopyranoside (G4G4G4G3G-MU, **1f**), were synthesized as reported previously (*14*, *15*). The inhibitor 3-*O*-β-cellotriosyl-D-glucopyranose (G4G4G3G, **2**) was obtained from enzymatic degradation of barley β-glucan by recombinant *B. licheniformis* 1,3-1,4-β-glucanase (*8*, *15*).

Site-Directed Mutagenesis by PCR. The gene coding for *B. macerans* 1,3-1,4-β-glucanase cloned into pTZ19R as a

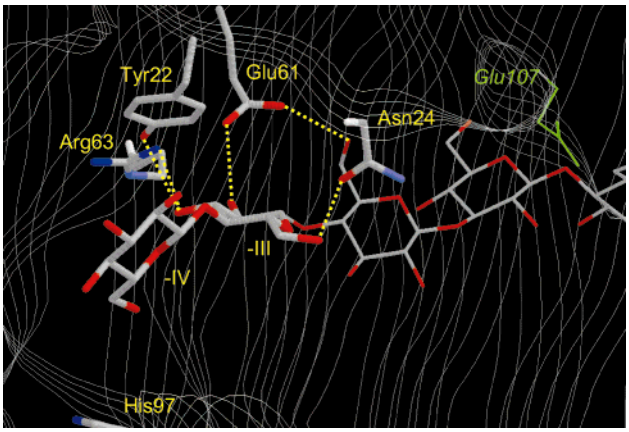

FIGURE 5: Structural model of protein−carbohydrate interactions at subsites −IV and III.

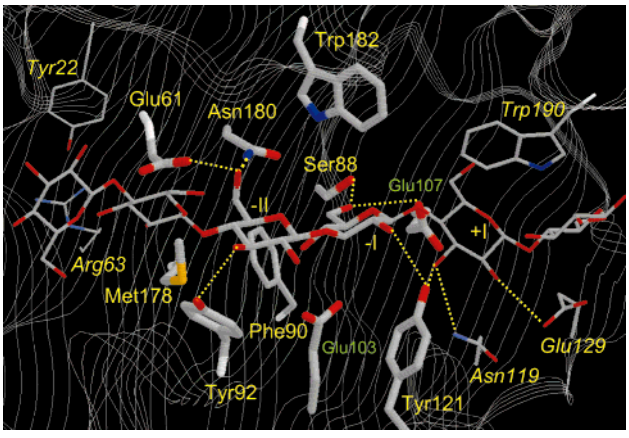

FIGURE 6: Structural model of protein−carbohydrate interactions at subsites −II, −I and +I.

0.85-kilobase EcoRI/HindIII fragment (*23*) was used as template for mutagenic polymerase chain reaction PCR, following the method of Landt et al. (*24*) in two separate steps. The first comprises the use of a mutagenic primer and one of the universal primers flanking the β-1,3-1,4-glucanase gene. The primers were the following: Y22A, 5′-CC CATTGGAGGCCCCATCTGC-3′; Y22F, 5′-CCCATTG-GAAAACCCATCTGC-3′; Y22W, 5′-CTTGTGGGGGGG-TAACCTGGTGGGTAGACGG-3′; N24A, 5′-CACCCCCC-

CCGCGGAATACCC-3′; N24Q, 5′-CTTGTGGGGGGGGA--CCCTTATGGG-3′; E61A, 5′-CTGCGCGGCCTACCGATCAACG-3′; E61D, 5′-GCGCGGATTACCGATC-3′; E61Q, 5′-GACTGCGCG CAGTACCGA-3′; R63K, 5′-CGTTGATTTGTACTCCGCG-3′; R63A, 5′-CGTTGATGCGT ACTCCGC-3′; S88A, 5′-GTCTCAGCCTTTTTCACG-3′; F90A, 5′-CTCATCCTTTGCCAC GTATAC-3′; Y92A, 5′-CTTTTTCACGGCTACAGGACC-3′; Y92W, 5′-CCTTTTTCACGTGGACAGGACCTGC-3′; H97R, 5′-ACAGGACCTGCTCGTGGCACAC-3′; H97D, 5′-ACA GGACCTGCTGATGGCACAC-3′; N119L, 5′-GTATAATAGAGAAACTGGAC-3′; N119D, 5′-GTCCAGTTTGACTATTATAC-3′; Y121F, 5′-GTTTAACTATTTTACCAATGG-3′; Y121A, 5′-GTTTAACTATGCTACCAATGG-3′; E129Q, 5′-TAACCTTTTGATGACCGC C-3′; H143A, 5′-TCTCTTGGCTTTGATGCATCAAAGGGCTTCGCAACCTATGCTTTCGATTGG-3′;N180A, 5′-CAAAATTATGATGGCTCTATGGAAC-3′; N180Q, 5′-ATGAT GCAGCTATGGAACGG-3′; W182Y, 5′-GATGAATCTATATAACGGAACC-3′ and W190A, 5′-GTGGATGACGCGTTAGGTTC-3′. The second step uses the product of the first PCR as a primer and the opposite universal primer to yield the full size 1,3-1,4-β-glucanase gene with the desired mutation. The final amplified DNA was digested with *Eco*RI and *Hin*dIII restriction enzymes, and the mutated gene fragment ligated back into the parental vector, pTZ19R. Plasmids with mutated genes were transformed into *E. coli* DH5α cells. Transformants were screened for β-glucanase activity on lichenan-agar plates (0.01% w/v lichenan), using the Congo red staining assay (*25*). Selected clones were verified by DNA sequencing of the entire gene using the standard direct (1224) and reverse (1221) primers (Pharmacia).

Purification of wt and Mutant Enzymes. Proteins were purified from cell extract of *E.coli* DH5α cultures harboring the mutagenized plasmids basically as described before (*26*, *27*). Purity was higher than 95% as judged by SDS−polyacrylamide gel electrophoresis according to Laemmli (*28*). Enzyme concentrations were determined by the Bradford protein assay (*29*) using bovine serum albumin as protein standard.

Enzyme Kinetics. (a) Kinetics with Lichenan. Enzyme-catalyzed hydrolysis was performed by incubating the substrate at appropriate concentrations (0.1−9 mg mL^{-1}) in citrate-phosphate buffer (6.5 mM citric acid and 87 mM Na_2HPO_4), pH 7.2, and 0.1 mM $CaCl_2$ in a thermostated bath at 50 °C. After 5 min of preincubation, reactions were initiated by adding the enzyme to a final concentration of 0.7 nM to 1.2 μM. Initial rates were obtained by determining the net release of reducing sugars at 1 min intervals for a total time of 5−10 min using 3,5-dinitrosalicilic acid reagent (*30*). Reducing power was expressed as equivalent glucose concentration, and rates were given in micromoles of glucose per minute milligrams.

(b) Kinetics with the 4-Methylumbelliferyl Glycosides. All kinetics were performed by following changes in UV absorbance due to the release of 4-methylumbelliferone, using 1 cm path-length cells in a Varian Cary 4E spectrophotometer with a Peltier temperature control system, which maintained the cells at 50 °C. The rates of the enzyme-catalyzed hydrolysis were determined by incubating the substrate at the appropriate concentration (0−10 mM) in citrate-phosphate buffer (6.5 mM citric acid and 87 mM Na_2HPO_4), pH 7.2, and 0.1 mM $CaCl_2$ for 5 min in a thermostated cell holder. Reactions were initiated by the addition of enzyme to a final concentration of 20 nM to 15 μM and monitoring the absorbance change at 365 nm ($\Delta\epsilon = 5356\ M^{-1}\ cm^{-1}$) (*16*). Concentration of stock solutions of **1a**−**e** were determined by UV spectrophotometry using the molar extinction coefficient reported for 4-methylumbelliferyl glycosides $\epsilon_{316nm} = 13\,600\ M^{-1}\ cm^{-1}$ (*31*). The molar extinction coefficients at the working wavelengths (355 nm for kinetics at pH <7, 365 nm for kinetics at pH ≥7) were $\epsilon_{355nm} = 265\ M^{-1}\ cm^{-1}$ and $\epsilon_{365nm} = 177\ M^{-1}\ cm^{-1}$ and were pH independent. The pH-dependent molar extinction coefficients of 4-methylumbelliferone (MU−OH) at 355 and 365 nm were taken from Malet and Planas (*16*).

(c) pH Dependence with 4-Methylumbelliferyl Trisaccharide. The kinetic parameters as a function of the pH for the enzyme-catalyzed hydrolysis of **1c** were determined as in point b in citrate-phosphate buffer (11 mM citric acid and 11 mM NaH_2PO_4), adjusting the pH at 50 °C to the required value with NaOH, and 0.1 mM $CaCl_2$ and keeping the ionic strength constant at 0.1 M with added KCl. The release of 4-methylumbelliferone was monitored at 355 nm for reactions at pH <7 and at 365 nm for reactions at pH ≥7, using the appropriate $\Delta\epsilon$ ($\epsilon_{MU-OH,\lambda} - \epsilon_{1c,\lambda}$) at each pH (*16*). k_{cat}/K_M values at each pH were calculated as the slope of the linear dependence of initial rates with substrate concentration in the range 0.015−0.3 mM.

(d) Inhibition Kinetics. Reaction conditions were similar to those for kinetics with the 4-methylumbelliferyl glycosides. Reaction mixtures contained the substrate (G4G3G-MU, **1c**) in concentrations 0.12, 0.17, 0.25, and 0.5 mM, and the inhibitor (G4G4G3G, **2**) in concentrations 0, 0.5, 1.0, 1.5, and 2.0 mM for wt and Y121F, 0, 0.7, 1.3, 2.0, 3.0, and 4.0 mM for S88A, and 0, 0.03, 0.05, 0.1, and 0.2 mM for Y121A. Enzymes were added to final concentrations of 50 nM for wt, 370 nM for S88A, 20 nM for Y121F, and 300 nM for Y121A. The K_I values were determined by nonlinear regression to the competitive inhibition model $v_0 = V_{max}\,[S]/([S] + K_M[1 + [I]/K_I])$, using "Micromath Scientist" software.

RESULTS

Design of the Mutations. Figure 2 shows the putative protein−carbohydrate interactions that are proposed by inspection of the modeled enzyme−substrate complex. In subsite −IV, only a stacking interaction with Tyr22 is observed. Subsites −III and −II may have extensive hydrogen-bonding interactions involving a number of residues: Tyr22, Asn24, Glu61, and Arg63 in subsite −III, and Glu61, Phe90, Tyr92, and Asn180 in subsite −II. Although not observed in the modeled complex, His97 may also interact with the substrate in subsite −III according to the X-ray structure of the H(A16M) enzyme-epoxyalkyl inhibitor (*21*). For subsite −I, the model might not be appropriate since ring distortion is expected for the bound glucopyranose unit bearing the glycosidic bond to be hydrolyzed, as proposed for other glycosidases (*32*, *33*). The current model places a $^4C_1$ chair conformation in this subsite for which the glycosidic bond to the glucose residue in subsite +I is strained into a conformation of about 3 kcal mol^{-1} above

Table 1: Activity of Wild-Type and Mutant 1,3-1,4-β-Glucanases on Lichenan[a]

enzyme	k_{cat} (s^{-1})	K_m (mg mL^{-1})	k_{cat}/K_m (mL mg^{-1} s^{-1})	$\Delta\Delta G^{\ddagger b}_{mut-wt}$ (kcal mol^{-1})
WT	1191 ± 53	0.45 ± 0.08	2656 ± 580	
Y22F	481 ± 31	2.19 ± 0.36	220 ± 51	1.59
Y22A	325 ± 32	3.85 ± 0.77	85 ± 25	2.20
Y22W	787 ± 22	0.14 ± 0.03	5507 ± 1135	−0.47
N24A	262 ± 28	4.70 ± 1.05	56 ± 18	2.47
N24Q	667 ± 51	3.70 ± 0.70	180 ± 48	1.72
E61A	4.25 ± 0.12	2.64 ± 0.21	1.61 ± 0.17	4.74
E61D	113 ± 9	4.85 ± 0.80	23.2 ± 5.6	3.03
E61Q	8.08 ± 0.32	1.47 ± 0.18	5.48 ± 0.89	3.95
R63A	811 ± 33	1.95 ± 0.21	415 ± 61	1.19
R63K	867 ± 44	1.52 ± 0.19	571 ± 101	0.98
S88A	324 ± 15	0.33 ± 0.05	968 ± 192	0.65
F90A	13.82 ± 0.30	1.59 ± 0.11	8.68 ± 0.78	3.66
Y92A	15.48 ± 0.67	2.54 ± 0.24	6.09 ± 0.84	3.89
Y92W	361 ± 15	0.57 ± 0.08	639 ± 114	0.91
H97R	147 ± 5	0.89 ± 0.08	165 ± 21	1.78
H97D	276 ± 13	0.26 ± 0.07	1050 ± 324	0.60
N119D	48.9 ± 2.0	1.64 ± 0.17	29.8 ± 4.4	2.87
N119L	1.35 ± 0.04	0.48 ± 0.05	2.79 ± 0.35	4.39
Y121F	627 ± 20	0.16 ± 0.04	3876 ± 987	−0.24
Y121A	40.4 ± 1.8	0.13 ± 0.04	319 ± 112	1.35
E129Q	302 ± 9	2.37 ± 0.20	128 ± 15	1.94
H143A	1056 ± 29	0.46 ± 0.05	2316 ± 292	0.09
N180Q	46.6 ± 2.6	2.85 ± 0.36	16.3 ± 3.0	3.26
N180A	5.85 ± 0.22	1.38 ± 0.18	4.24 ± 0.73	4.12
W182Y	164 ± 8	0.68 ± 0.12	239 ± 54	1.54
W190A	40.5 ± 1.9	3.13 ± 0.33	12.9 ± 2.0	3.41

[a] Conditions: 6.5 mM citrate−87 mM phosphate buffer, pH 7.2, 0.1 mM $CaCl_2$, 50 °C. [b] $\Delta\Delta G^{\ddagger}_{mut-wt} = -RT \ln[(k_{cat}/K_M)_{mut}/(k_{cat}/K_M)_{wt}]$.

the global energy minimum for a relaxed β-1,4 glycosidic bond (*22*). The observed protein−carbohydrate contacts in this model involve Ser88, Glu109, and Tyr121, but other interactions may hold if ring distortion occurs upon binding. Subsite +I contains Asn119, Glu129, Tyr121, and Trp190 as residues interacting with the substrate. Finally, the glucopyranose unit in subsite +II is not hydrogen bonded to the enzyme in this model.

Different mutants have been designed to evaluate hydrogen bonding and hydrophobic (stacking) interactions. For hydrogen-bonding residues (Asn, Glu, Arg, His, and Ser), mutation to Ala will remove the interaction, and other mutations such as Asn → Gln, Glu → Asp, and Arg → Lys will conserve the functional side-chain group but modify or remove the interaction as a consequence of the larger or shorter side chain. Tyrosines are mutated to Phe, Ala and Trp; Tyr → Phe will remove a putative hydrogen bond interaction with an OH group of the substrate, and a further mutation Tyr → Ala will also eliminate any stacking interaction with a glucopyranose ring of the substrate, whereas a Tyr → Trp mutation introduces a larger volume but may maintain stacking interactions. The complete set of mutants prepared and analyzed in this work are listed in Tables 1 and 2. They were prepared by PCR site-directed mutagenesis, and the mutant proteins were purified to >95% purity as judged by SDS−polyacrylamide gel electrophoresis.

Activity on Lichenan. The mutants were first assayed for activity with the natural polysaccharide substrate lichenan under the same experimental conditions used later with the chromogenic oligosaccharide substrates. Michaelis−Menten parameters are given in Table 1. All the mutants, except Y22W and Y121F, are less active than the wild-type enzyme in terms of k_{cat}/K_M values. K_M values are higher (only in few cases equal) than that for the wild-type enzyme, consistent with the involvement of the mutated residues in substrate binding.

Kinetics with 4-Methylumbelliferyl Glycosides. Kinetics of the enzymatic reactions were determined in citrate/phosphate buffer at pH 7.2 and 50 °C. While the optimal temperature for the wild-type enzyme is 65 °C, some mutants were more thermolabile, and 50 °C was the highest temperature at which all mutants were stable during the activity assays. The chromogenic substrates $(G4)_nG3G$-MU (**1b**−**e**, $n = 0-3$, MU = 4-methylumbelliferyl) underwent a single glycosidic bond cleavage upon enzymatic hydrolysis with release of the 4-methylumbelliferone aglycon. Initial velocities at different substrate concentrations were fitted to eq 1

$$v = \frac{k_{cat}[E]_0[S]}{K_M + [S]} \quad (1)$$

$$v = \frac{k_{cat}[E]_0[S]}{K_M + [S] + ([S]^2/K_1)} \quad (2)$$

(Michaelis−Menten model) in most of the cases, except for some mutants where inhibition at high substrate concentration was observed and data were fitted to eq 2 (Michaelis−Menten with substrate inhibition model). This behavior has been already observed for the highly homologous *Bacillus licheniformis* 1,3-1,4-β-glucanase with chromogenic low molecular weight oligosaccharides substrates (*16*); at high substrate concentration, binding of a second molecule of substrate produces unproductive ternary complexes $E{\cdot}S_2$.

In general, the best fit depends on the relative values of K_M and K_I; if $2K_M \leq [S]_{max} \leq 0.1K_I$, where $[S]_{max}$ is the highest substrate concentration assayed, then the regular Michaelis−Menten model (eq 1) was used.

Kinetic parameters for the wild-type and mutant enzymes are summarized in Table 2. k_{cat} values range from 6×10^{-4} to 1.8 s^{-1} for the trisaccharide substrate **1c**, a spread of 3×10^4-fold and from 2×10^{-3} to 6 s^{-1} for the tetrasaccharide **1d**. k_{cat}/K_M values were calculated from the individual k_{cat} and K_M parameters when the highest substrate concentration assayed was greater than $2K_M$ or evaluated as the slope of the linear region of v_0 vs [S] at low substrate concentration when no saturation was reached ($[S]_{max} < 2K_M$).

Disaccharide Kinetics. Substrate **1b** (G3G-MU) showed more complex kinetics than the higher homologues **1c**−**e**, not fulfilling the Michaelis−Menten model. After mixing enzyme and substrate, the change in absorbance due to the release of the chromophoric aglycon was not linear at initial reaction times; a long lag in the progress curve (Abs vs time) with an upward curvature (activation phase) was observed for the first 1−2% of substrate conversion, followed by a linear progress curve (steady-state phase) up to 5−10% conversion. The dependence of the steady-state rate with substrate concentration was not hyperbolic, rather a sigmoidal curve with enzyme activation at low substrate concentration was obtained. As an example, Figure 3 shows the v_0 vs [**1b**] plot for the wt enzyme. The kinetic model which best accounts for this behavior (Scheme 2) considers that, once the productive E·S complex is formed, a second molecule

Table 2: Kinetic Parameters for Wild-Type 1,3-1,4-β-Glucanase and Mutants at Subsites −IV and −III with Substrates **1c**−**e**[a]

mutant	substrate	kinetic model[b]	[S] (mM)	k_{cat} (s^{-1})	K_M (mM)	k_{cat}/K_M[c] (M^{-1} s^{-1})
WT	G-MU		0.5−13	nd	nd	0.54 ± 0.02 *
	G4G3G-MU	A	0.05−5	1.83 ± 0.09	1.96 ± 0.22	(9.36 ± 0.64) × 10^2
	$(G4)_2$G3G-MU	A	0.1−3.5	3.84 ± 0.13	0.55 ± 0.06	(7.02 ± 0.54) × 10^3
	$(G4)_3$G3G-MU	B	0.1−3	3.97 ± 0.34	0.53 ± 0.08	(7.57 ± 0.53) × 10^3
H143A	G4G3G-MU	B	0.02−4	1.52 ± 0.08	1.98 ± 0.15	(7.67 ± 0.19) × 10^2
	$(G4)_2$G3G-MU	B	0.05−2	5.07 ± 0.15	0.64 ± 0.03	(7.93 ± 0.15) × 10^3
subsites −IV, −III						
Y22F	G4G3G-MU	B	0.06−9	0.23 ± 0.01	5.46 ± 0.32	(4.16 ± 0.07) × 10^1
	$(G4)_2$G3G-MU	A	0.05−7	1.19 ± 0.02	4.00 ± 0.10	(3.00 ± 0.04) × 10^2
	$(G4)_3$G3G-MU		0.1−0.4	nd	nd	(3.00 ± 0.04) × 10^2 *
Y22A	G4G3G-MU	B	0.1−12	0.12 ± 0.01	5.23 ± 0.58	(2.29 ± 0.09) × 10^1
	$(G4)_2$G3G-MU	A	0.1−9	0.38 ± 0.01	6.05 ± 0.4	(5.35 ± 0.18) × 10^1 *
	$(G4)_3$G3G-MU		0.1−0.4	nd	nd	(5.74 ± 0.08) × 10^1 *
Y22W	G4G3G-MU	B	0.1−14	2.70 ± 0.26	2.86 ±0.43	(9.43 ± 0.56) × 10^2
	$(G4)_2$G3G-MU	A	0.04−2	5.76 ± 0.4	0.23 ±0.02	(2.52 ± 0.16) × 10^4
	$(G4)_3$G3G-MU	B	0.02−2	5.33 ± 0.28	0.09 ±0.01	(5.93 ± 0.63) × 10^4
N24A	G4G3G-MU	A	0.5−15	(4.2 ± 0.2) × 10^{-2}	14 ± 1	2.92 ± 0.07 *
	$(G4)_2$G3G-MU	A	0.1−9	0.33 ± 0.02	13 ± 1	(2.39 ± 0.04) × 10^1 *
	$(G4)_3$G3G-MU		0.1−2	nd	nd	(2.52 ± 0.04) × 10^1 *
N24Q	G4G3G-MU	A	0.1−17	0.046 ± 0.001	7.67 ± 0.46	5.94 ± 0.21
	$(G4)_2$G3G-MU	A	0.2−6	0.28 ± 0.01	7.32 ± 0.46	(3.61 ± 0.01) × 10^1 *
	$(G4)_3$G3G-MU		0.2−1	nd	nd	(7.34 ± 0.18) × 10^1 *
E61A	G4G3G-MU	A	0.15−11	(4.1± 0.2) × 10^{-4}	10.0 ± 0.7	(3.84 ± 0.13) × 10^{-2} *
	$(G4)_2$G3G-MU	A	0.2−5	(3.6 ± 0.5) × 10^{-3}	6.7 ±1.4	0.52 ± 0.07 *
E61D	G4G3G-MU	A	0.3−16	(8.7 ± 0.4) × 10^{-3}	5.83 ± 0.60	1.49 ± 0.09
	$(G4)_2$G3G-MU	A	0.3−6	(6.2 ± 0.4) × 10^{-2}	5.50 ± 0.54	(1.05 ± 0.04) × 10^1 *
E61Q	G4G3G-MU	A	0.03−10	(1.04 ± 0.02) × 10^{-3}	3.88± 0.14	0.27 ± 0.06
	$(G4)_2$G3G-MU	A	0.1−4	(2.24 ± 0.03) × 10^{-3}	0.98 ± 0.04	2.29 ± 0.13
R63A	G4G3G-MU	A	0.1−7	(2.44 ± 0.01) × 10^{-1}	3.27 ± 0.24	(7.47 ± 0.30) × 10^1
	$(G4)_2$G3G-MU		0.1−1.3	nd	nd	(2.30 ± 0.05) × 10^2 *
R63K	G4G3G-MU	A	0.3−11	(2.01 ± 0.08) × 10^{-1}	2.51 ± 0.27	(8.01 ± 0.59) × 10^1
	$(G4)_2$G3G-MU		0.1−1	nd	nd	(3.67 ± 0.03) × 10^2 *
H97R	G4G3G-MU	B	0.02−9	(8.67 ± 0.35) × 10^{-2}	2.55 ± 0.18	(3.40 ± 0.10) × 10^1
	$(G4)_2$G3G-MU	A	0.04−4	(7.51 ± 0.07) × 10^{-1}	2.77 ± 0.05	(2.53 ± 0.02) × 10^2 *
H97D	G4G3G-MU	A	0.04−4	(6.19 ± 0.12) × 10^{-1}	2.71 ±0.09	(2.28 ± 0.04) × 10^2
	$(G4)_2$G3G-MU	B	0.01−5	2.57 ± 0.07	2.19 ±0.08	(1.17 ± 0.02) × 10^3
subsite −II						
F90A	G4G3G-MU	A	0.2−10	(2.19 ± 0.08) × 10^{-3}	3.72 ± 0.32	0.59 ± 0.03
	$(G4)_2$G3G-MU	A	0.1−6	(1.82 ± 0.02)· 10^{-2}	4.11 ± 0.10	3.91 ± 0.04 *
Y92W	G4G3G-MU	A	0.02−5	(2.30 ± 0.11) × 10^{-1}	2.64 ± 0.24	(8.69 ± 0.43) × 10^1
	$(G4)_2$G3G-MU	A	0.02−4	1.53 ± 0.02	2.38 ± 0.06	(6.44 ± 0.09) × 10^2
N180Q	G4G3G-MU	A	0.2−15	(1.75 ± 0.10) × 10^{-3}	7.24 ± 0.84	0.24 ± 0.01
	$(G4)_2$G3G-MU		0.06−9	nd	nd	1.44 ± 0.03 *
N180A	G4G3G-MU	A	0.1−10	(6.21 ± 0.41) × 10^{-4}	3.35 ± 0.49	0.19 ± 0.02
	$(G4)_2$G3G-MU	A	0.1−7	(4.13 ± 0.09) × 10^{-3}	2.34 ± 0.11	1.76 ± 0.05
W182Y	G4G3G-MU	A	0.2−10	(2.95 ± 0.08) × 10^{-2}	10.4 ± 0.5	2.57 ± 0.06 *
	$(G4)_2$G3G-MU	A	0.1−7	(1.76 ± 0.02) × 10^{-1}	5.69 ± 0.11	(2.99 ± 0.02) × 10^1 *
subsite −I						
S88A	G4G3G-MU	B	0.2−8	(2.31 ± 0.19) × 10^{-1}	1.33 ± 0.19	(1.74 ± 0.11) × 10^2
Y121F	G4G3G-MU	B	0.1−5	1.35 ± 0.16	0.58 ± 0.12	(2.35 ± 0.25) × 10^3
Y121A	G4G3G-MU	B	0.1−8	(2.35 ± 0.18) × 10^{-1}	3.71 ± 0.41	(6.34 ± 0.24) × 10^1
subsite +I						
N119D	G4G3G-MU	A	0.5−5	(4.52 ± 0.13) × 10^{-1}	1.79 ± 0.13	(2.53 ± 0.12) × 10^2
N119L	G4G3G-MU	B	0.1−5	(1.80 ± 0.10) × 10^{-1}	0.43 ± 0.05	(4.15 ± 0.28) × 10^2
E129Q	G4G3G-MU	B	0.5−7	1.58 ± 0.06	1.78 ± 0.12	(8.86 ± 0.27) × 10^2
W190A	G4G3G-MU	B	0.3−7	(9.21 ± 0.65)·10^{-1}	3.24 ± 0.34	(2.84 ± 0.10) × 10^2

[a] Conditions: 6.5 mM citrate-87 mM phosphate buffer, pH 7.2, 0.1 mM $CaCl_2$, 50 °C. [b] Kinetic model: A, Michaelis−Menten (eq 1); B, Michaelis−Menten with substrate inhibition (eq 2). [c] k_{cat}/K_M calculated from individual k_{cat} and K_M values, except in those cases (*) for which it is calculated as the slope of the linear region v_0 vs [S] at low substrate concentration (see text). nd, not determined.

Scheme 2: Model for Activation Kinetics of 1,3-1,4-β-Glucanases with the Disaccharide Substrate **1b**

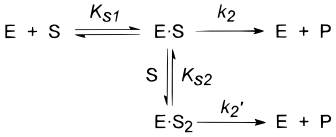

of substrate is able to bind with higher affinity to form a kinetically competent ternary complex (E·S_2). Data were properly fitted by eq 3, which describes the proposed kinetic model.

$$\frac{v}{[E]_0} = \frac{k_2[S] + k_2'\dfrac{[S]^2}{K_{S2}}}{K_{S1} + [S] + \dfrac{[S]^2}{K_{S2}}} \qquad (3)$$

Table 3: Kinetic Parameters for the Hydrolysis of the Disaccharide Substrate **1b** by Wild-Type and Mutant 1,3-1,4-β-Glucanases[a]

mutant	kinetic model[b]	k_2 (s^{-1})	K_{S1} (mM)	K_{S2} (mM)	k_2K_{S1} (M^{-1} s^{-1})	$\Delta\Delta G^{\ddagger}_{mut-wt}$ (**1b**) (kcal mol)$^{-1}$
WT	C	$(4.07 \pm 0.05) \times 10^{-2}$	14.7 ± 1.3	1.99 ± 0.32	2.77 ± 0.27	
H143A	C	$(3.59 \pm 0.07) \times 10^{-2}$	12.6 ± 0.6	2.23 ± 0.27	2.85 ± 0.18	-0.02
subsites −IV, −III						
Y22F	C	$(2.78 \pm 0.04) \times 10^{-2}$	13.2 ± 0.3	2.34 ± 0.18	2.11 ± 0.08	$+0.17$
Y22A	C	$(6.78 \pm 0.08) \times 10^{-3}$	11.3 ± 0.2	3.24 ± 0.23	0.60 ± 0.02	$+0.98$
Y22W	C	$(6.71 \pm 0.12) \times 10^{-2}$	13.7 ± 1.1	1.48 ± 0.24	4.90 ± 0.48	-0.36
N24Q	C	$(5.65 \pm 0.15) \times 10^{-4}$	10.9 ± 0.6	2.91 ± 0.48	0.052 ± 0.004	$+2.54$
N24A	C	$(2.74 \pm 0.08) \times 10^{-3}$	11.1 ± 0.3	5.41 ± 0.73	0.25 ± 0.01	$+1.54$
E61D	nd[c]					
E61A	A	$(5.97 \pm 0.34) \times 10^{-5}$	2.12 ± 0.33		0.028 ± 0.006	$+2.94$
E61Q	A	$(4.27 \pm 0.24) \times 10^{-4}$	5.96 ± 0.62		0.072 ± 0.011	$+2.33$
R63K	C	$(2.56 \pm 0.04) \times 10^{-2}$	12.9 ± 0.6	2.22 ± 0.24	1.98 ± 0.11	$+0.21$
R63A	C	$(2.80 \pm 0.04) \times 10^{-2}$	14.6 ± 0.9	1.62 ± 0.20	1.92 ± 0.14	$+0.23$
H97R	C	$(1.46 \pm 0.04) \times 10^{-2}$	9.28 ± 0.30	4.48 ± 0.68	1.57 ± 0.09	$+0.36$
H97D	C	$(2.87 \pm 0.07) \times 10^{-2}$	12.7 ± 1.0	2.19 ± 0.43	2.26 ± 0.24	$+0.13$
subsite −II						
F90A	C[d]	$(6.06 \pm 0.80) \times 10^{-5}$	24 ± 20	nd	$(1.4 \pm 1.0) \times 10^{-3}$	$+4.85$
F92W	C	$(8.24 \pm 0.09) \times 10^{-3}$	15.4 ± 0.8	1.51 ± 0.15	0.53 ± 0.03	$+1.06$
N180Q	C[d]	$(5.05 \pm 0.27) \times 10^{-5}$	25 ± 13	nd	$(2.0 \pm 1.0) \times 10^{-3}$	$+4.63$
N180A	C[d]	$(8.47 \pm 0.73) \times 10^{-5}$	4.5 ± 4	nd	$(3.8 \pm 3.0) \times 10^{-4}$	$+5.69$
W182Y	C	$(1.79 \pm 0.34) \times 10^{-4}$	35 ± 11	2.5 ± 2.1	$(5.1 \pm 2.6) \times 10^{-3}$	$+4.03$
subsite −I						
S88A	C	$(7.53 \pm 0.14) \times 10^{-3}$	13.0 ± 0.3	3.48 ± 0.32	0.58 ± 0.03	$+1.00$
Y121F	C	$(1.22 \pm 0.02) \times 10^{-1}$	17 ± 5	0.35 ± 0.13	7.1 ± 2.1	-0.60
Y121A	nd[c]					

[a] Conditions: 6.5 mM citrate−87 mM phosphate buffer, pH 7.2, 0.1 mM $CaCl_2$, 50 °C. [b] Kinetic model: A, Michaelis−Menten (eq 1); C, substrate activation model (eq 4). [c] Kinetic parameters not determined since v_0 was not linear with enzyme concentration at constant [S]. [d] Fitting to eq 4 gave interparameter correlation between K_{S1} and K_{S2}. k_2/K_{S1} was calculated by fitting the data at low substrate concentration to the simplified equation $v_0/[E]_0 = (k_2/K_{S1})[S]+(k_2/K_{S1}\cdot K_{S2})[S]^2$.

However, k_2 and $k_{2'}$ values were very similar and fitting was improved when considering $k_2 = k_{2'}$, so the simplified eq 4 gave the best results.

$$\frac{v}{[E]_0} = \frac{k_2[S](1 + [S]/K_{S2})}{K_{S1} + [S] + [S]^2K_{S2}} \quad (4)$$

According to this kinetic model, the second-order rate constant k_2/K_{S1} describes the process through the productive binary complex (E·S), and it is then comparable to the k_{cat}/K_M parameter of normal Michaelis−Menten kinetics. Steady state parameters are given in Table 3. Only mutants at position 61 (E61D,A) showed normal Michaelis−Menten kinetics.

pH Dependence of k_{cat}/K_M. The steady-state values of k_{cat}/K_M for wild-type and mutants at subsite −I (S88A, Y121F, and Y121A) with the trisaccharide substrate **1c** were measured over a pH range of 4.5−9 in citrate-phosphate buffer and constant ionic strength (100 mM) with added KCl at 50 °C. The pH dependence of k_{cat}/K_M for each enzyme follows a bell-shaped curve corresponding to a double-ionization process. The pH profiles are plotted in Figure 4 as $\log(k_{cat}/K_M)$ vs pH. Kinetic pK_a and limiting k_{cat}/K_M values were obtained from nonlinear regression fitting of the data to eq 5 . Results are summarized in Table 4.

$$\frac{k_{cat}}{K_M} = \frac{(k_{cat}/K_M)_{lim}}{1 + 10^{pK_{a1}-pH} + 10^{pK-pH_{a2}}} \quad (5)$$

Inhibition Kinetics. Subsite −I mutants were also analyzed for ligand binding through inhibition kinetics with the tetrasaccharide **2** (G4G4G3G, Scheme 1), one of the final oligosaccharide products from barley β-glucan degradation by 1,3-1,4-β-glucanases. Compound **2** was a competitive inhibitor of the enzyme-catalyzed hydrolysis of **1c** by the wt and mutant enzymes. Inhibition constants are given in Table 5, together with the overall effect of each mutation on binding energy, calculated as

$$\Delta\Delta G^b = -RT \ln[(K_I)_{mut}/(K_I)_{wt}] \quad (6)$$

Table 4: Kinetic pK_a Values on k_{cat}/K_M for Substrate **1c** of Wild-Type 1,3-1,4-β-Glucanase and Mutants at Subsite −I[a]

mutant	$(k_{cat}/K_M)_{lim}$ (M^{-1} s^{-1})	pK_{a1}	pK_{a2}
WT	3022 ± 126	5.51 ± 0.05	6.91 ± 0.05
S88A	624 ± 29	5.50 ± 0.05	6.90 ± 0.05
Y121F	8112 ± 107	5.58 ± 0.02	6.85 ± 0.02
Y121A	310 ± 25	5.74 ± 0.07	6.85 ± 0.02

[a] Conditions: 11 mM citrate−11 mM phosphate buffer, pH 4.5−9, 0.1 mM $CaCl_2$, I = 100 mM (with added KCl), 50 °C. The pH dependence of (k_{cat}/K_M) is shown in Figure 5. pK_a and $(k_{cat}/K_M)_{lim}$ values are derived by fitting to eq 5.

Table 5: Inhibition Constants for Wild-Type and Subsite −I Mutant 1,3-1,4-β-Glucanases with the Competitive Inhibitor G4G4G3G (**2**)[a]

mutant	K_I(mM)	$\Delta\Delta G^b$ (kcal mol^{-1})
wt	1.12 ± 0.03	
S88A	3.15 ± 0.09	$+0.66$
Y121F	1.04 ± 0.03	-0.05
Y121A	0.113 ± 0.003	-1.47

[a] Conditions: citrate-phosphate buffer, pH 7.2, 0.1 mM $CaCl_2$, 50 °C. Substrate **1c**: 0.1−0.5 mM. Inhibitor **2**: 0−2 mM. $\Delta\Delta G^b$ values relative to the wild-type enzyme are calculated according to eq 6.

Scheme 3: Thermodynamic Cycle Model

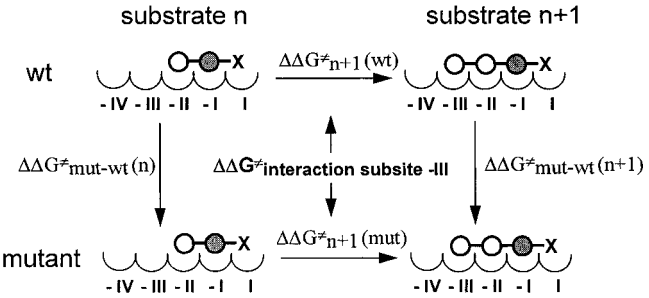

DISCUSSION

Subsite Mapping of the Wild-Type Enzyme. The analysis previously developed for the *B. licheniformis* 1,3-1,4-β-glucanase (*16*) was applied to map the subsites on the nonreducing end from the scissile glycosidic bond in the *B. macerans* wild-type enzyme. The contribution of single subsites to transition-state stabilization are calculated from the second-order rate constants k_{cat}/K_M for the series of homologous substrates **1a**−**e** according to

$$\Delta\Delta G^{\ddagger}_{subsite} = \Delta G^{\ddagger}_{n+1} - \Delta G^{\ddagger}_{n} = -RT \ln\{(k_{cat}/K_M)_{n+1}/(k_{cat}/K_M)_n\} \quad (7)$$

where n and n+1 are two homologous substrates differing in one glucopyranose unit, and $\Delta\Delta G^{\ddagger}$ is assigned to subsite n+1. Calculated values are (kcal mol^{-1}): 1.05 (subsite −II), 3.72 (subsite −III), 1.29 (subsite −IV). They are essentially identical to those reported for the *B. licheniformis* enzyme from kinetics with the same substrates. Although the *B. macerans* enzyme is slightly less active (∼80% in terms of k_{cat}/K_M for substrates **1a**−**e**), the relative distribution of subsites is the same as expected for these highly homologous proteins, with subsite −III having the largest contribution to transition state stabilization.

Subsite Mapping Model for the Mutational Analysis: Thermodynamic Cycles. When comparing the wild-type and the mutant with the same substrate, the overall effect of the mutation to transition-state stabilization is given by

$$\Delta\Delta G^{\ddagger}_{mut-wt} = -RT \ln\{(k_{cat}/K_M)_{mut}/(k_{cat}/K_M)_{wt}\} \quad (8)$$

However, the measured effect may not only be the consequence of removing the interaction with the substrate, but also the result of any conformational change induced by the mutation that can have an indirect effect on activity. A thermodynamic cycle approach is proposed here (Scheme 3) to isolate the free energy of interaction from the overall effect (interaction plus conformational). Lets consider a residue that interacts with the substrate in subsite n + 1 (subsite −III in Scheme 3). Both the wild-type and the mutant at this residue are kinetically characterized with two chromogenic substrates of different length: substrate n + 1 that will occupy subsite n + 1, and a shorter substrate n, which leaves the mutated subsite empty in the productive complex. The transition-state stabilization energies $\Delta\Delta G^{\ddagger}$ are calculated from k_{cat}/K_M values for each reaction (eqs 7 and 8) to build the thermodynamic cycle that relates them. Ideally, no difference between wild-type and mutant would be expected for substrate n, since the subsite where the mutation has been introduced remains empty. So, $\Delta\Delta G^{\ddagger}_{mut-wt}(n)$ is the "background" effect that accounts for small solvent and structural rearrangements introduced by the mutation (conformational effect), and it is assumed constant for both substrates, n and n + 1. Then, the $\Delta\Delta G^{\ddagger}$ assigned to the individual interaction in subsite n + 1 will be the difference of $\Delta\Delta G^{\ddagger}_{mut-wt}$ between both substrates, or what is the same, the difference between the contribution of subsite n + 1 to transition state stabilization in the mutant and the wild-type:

$$\Delta\Delta G^{\ddagger}_{interaction} = \Delta\Delta G^{\ddagger}_{n+1}(mut) - \Delta\Delta G^{\ddagger}_{n+1}(wt) \quad (9)$$

Mutant H143A was constructed as a control mutation to test the effect of an amino acid replacement far away from the binding cleft on the kinetic parameters and establish the limit and sensitivity of the subsite mapping approach. When applying the above model to wild-type and H143A with substrates **1b**−**d** (Table 6), a $\Delta\Delta G^{\ddagger}$ of 0.1−0.2 kcal mol^{-1} is calculated for subsites −III and −IV. Thus, values of $\Delta\Delta G^{\ddagger}_{interaction} \leq 0.2$ kcal mol^{-1} are not assignable to any specific interaction.

Table 6: Contribution to Transition-State Stabilization of Protein−Carbohydrate Interactions in Subsites −IV and −III According to the Thermodynamic Cycles Model

		$\Delta\Delta G^{\ddagger}_{interaction}$ (kcal mol)$^{-1}$		
	mutant	−III	−IV	(−V)
His143	H143A	+0.15	−0.20	
Tyr22	Y22F	+1.82	+0.03	+0.05
	Y22A			
	F22A	−0.42	+0.72	−0.05
	Y22W	+0.36	−0.81	−0.50
Asn24	N24A	+2.15	+0.06	+0.02
	N24Q	+0.69	+0.14	
Glu61	E61A	+3.52	−0.38	
	E61D	+1.76	+0.26	
	E61Q	+2.88	−0.08	
Arg63	R63A	+1.38	+0.57	
	R63K	+1.36	+0.32	
His97	H97R	+1.76	+0.01	
	H97D	+0.77	+0.24	

Subsites −IV and −III. Figure 5 illustrates the interactions in the modeled enzyme−substrate complex. Different mutations for Tyr22, Asn24, Glu61, Arg63, and His97 are analyzed. Kinetic comparison of mutants and wt with the disaccharide **1b**, evaluated as $\Delta\Delta G^{\ddagger}_{mut-wt}$(**1b**), gives a measure of the background (nonspecific) effects of the mutations. They are negligible for substitutions at residues located in a β-sheet of the protein sandwich structure (R63 and H97) whereas those at loop residues (Y22 and N24) are significant (Table 3, right column). Glu61 should be treated differently because it also interacts with the Glc*p*-II. Although not assignable to any specific interaction, these results are in agreement with the larger flexibility of the loop and the more rigid structure of the β-sheet as part of the protein core.

Kinetics with trisaccharide (**1c**) and disaccharide (**1b**) substrates will give the energetic contribution to TS stabilization of the mutated residue in subsite −III, whereas the contribution in subsite −IV will be obtained from tetra (**1d**) and trisaccharide (**1c**) kinetics. Penta (**1e**) and tetrasaccharide (**1d**) data will provide information on an eventual new subsite −V, only when analyzing residues that are at the edge of

the binding site cleft on the nonreducing end. The calculated energetic contributions according to the thermodynamic cycle model are summarized in Table 6.

Tyr22. The phenolic side chain hydrogen-bonds with the 3-OH of glucopyranose in subsite −III, and has a stacking interaction with the glucopyranose ring in subsite −IV. Removal of the phenolic hydroxyl group by mutation to phenylalanine (Y22F) has a destabilizing effect on subsite −III and a negligible effect on subsite −IV. The 1.8 kcal mol^{-1} are then assigned to the H-bond Tyr22-OH···3-OH-(Glc*p*-III). A further mutation to alanine (F22A) gives an additional destabilization of 0.7 kcal mol^{-1} in subsite −IV, a value assigned to the lost stacking interaction with Glc*p*-IV. However, a stabilization of 0.4 kcal mol^{-1} is obtained for subsite −III in the Ala mutant relative to the Phe mutant. Since the hydrogen bond is absent in both mutations, this apparent stabilization may indicate that the aromatic side chain had unfavorable contacts with the substrate or that small structural rearrangements induced by the Phe to Ala mutation allows better binding to subsite −III. In fact, it is a consequence of a larger decrease in k_{cat}/K_M for the disaccharide substrate **1b** in the Y22A than in the Y22F mutant, whereas only a 2-fold reduction in catalytic efficiency is obtained for the trisaccharide **1c** (Tables 2 and 3). Therefore, it is more likely that the Y22A mutation causes a detrimental conformational change with the disaccharide because subsite −III remains empty, but the catalytic efficiency is partially recovered upon binding the additional Glc*p* unit of the trisaccharide. On the other hand, introduction of a larger aromatic ring (Y22W) has interesting effects: (a) the indolic nitrogen seems to maintain partially the hydrogen bond interaction with the 3-OH of Glc*p*-III, since the destabilization at subsite −III is only 0.36 kcal mol^{-1} as compared to the effect of Tyr to Phe mutation (1.8 kcal mol^{-1}); (b) the stacking interaction in subsite −IV is improved (−0.8 kcal mol^{-1} relative to the wt enzyme); and (c) the higher activity (in terms of k_{cat}/K_M) of the tryptophan mutant with a pentasaccharide substrate reflects a stabilizing effect of 0.5 kcal mol^{-1} for a virtual subsite −V, suggesting that the larger aromatic side chain of the Trp residue is able to interact with an additional glucopyranose ring, as a new subsite −V had been created. Overall, the Y22W mutant maintains the same catalytic efficiency (k_{cat}/K_M) with di- and trisaccharide substrates compared to the wt protein, but it is a better enzyme for the hydrolysis of larger substrates (tetra- and pentasaccharides). Likewise, it shows higher catalytic efficiency than the wt enzyme with the polymeric substrate lichenan (Table 1).

Asn24. The side-chain amide group of Asn24 hydrogen bonds with the 6-OH of Glc*p*-III, with a contribution of 2.2 kcal mol^{-1} to TS stabilization (N24A mutant, Table 6). Keeping the functional group but introducing a larger side chain (N24Q) seems to maintain partially the hydrogen bond interaction as seen by the lower destabilizing effect in subsite −III (0.7 as compared to 2.2 kcal mol^{-1}).

Glu61. The γ-carboxylate of Glu61 forms a bidentate hydrogen-bond with the 2-OH group of Glc*p*-III and the 6-OH of Glc*p*-II. The $\Delta\Delta G^{\ddagger}$ of 3.5 kcal mol^{-1} for the mutation E61A corresponds to the contribution of the H-bond between the 2-OH of Glc*p*-III and the charged γ-carboxylate; the interaction in subsite −II is not included according to the thermodynamic cycles model since it is also absent with the reference disaccharide substrate **1b**. Mutation to Gln does not change the size of the side chain but replaces a charged for an uncharged residue, with a destabilizing effect of 2.9 kcal mol^{-1}. These large values indicate that Glu61 is an important residue in defining the specificity for a cellobiosyl unit in subsites −III and −II as it will be discussed later.

Table 7: Effects on Transition-State Stabilization of Mutations at Subsites −II, −I, and +I

		$\Delta\Delta G^{\ddagger}_{wt-mut}$ (kcal mol) substrate^{-1}		
	mutant	**1b**	**1c**	**1d**
His143	H143A	−0.02	+0.13	−0.03
subsite −II				
Glu61	E61A	+2.94	+6.46	+6.08
	E61Q	+2.33	+5.21	+5.13
	E61D		+4.12	+4.16
Phe90	F90A	+4.85	+4.71	+4.79
Tyr92	Y92W	+1.06	+1.53	+1.53
Asn180	N180A	+5.69	+5.44	+5.30
	N180Q	+4.63	+5.29	+5.43
Trp182	W182Y	+4.18	+3.77	+3.49
subsite −I				
Ser88	S88A	+1.00	+1.08	
Tyr121	Y121F	−0.60	−0.59	
	Y121A		+1.72	
subsite +I				
Asn119	N119D		+0.84	
	N119L		+0.52	
Glu129	E129Q		+0.04	
Trp190	W190A		+0.76	

Arg63. Shortening the arginine side chain by mutation to lysine eliminates the hydrogen bond interaction with the 3-OH of Glc*p*-III (1.36 kcal mol^{-1}) and has no effect on subsite −IV. A further mutation to Ala does not introduce any additional change in subsite −III, but apparently the larger cavity has a destabilizing effect on subsite −IV.

His97. No interaction with the substrate is proposed in the modeled E·S structure [distance between NE2 and 2-OH-(Glc*p*-III) about 10 Å], but the histidine side chain rearranges toward the substrate in the X-ray structure of the covalent enzyme−inhibitor complex to form a hydrogen bond with the 2-OH(Glc*p*-III) (2.84 Å). Mutation to Arg (H97R) eliminates the interaction with a destabilization of 1.8 kcal mol^{-1} at subsite −III, and no effect on subsite −IV. Other *Bacillus* 1,3-1,4-β-glucanases have a carboxylic amino acid residue (Asp or Glu) in this position (see below), so the mutation H97D was analyzed. As compared to wild-type, the Asp mutation introduces only 0.8 kcal mol^{-1} destabilization in subsite −III, and again no effect on subsite −IV, suggesting that the Asp residue is able to maintain partially the H-bond assigned to His97.

Subsite −II. The complete analysis based on thermodynamic cycles used for subsites −IV and −III cannot be applied to subsite −II. It would require determination of the kinetic parameters with the disaccharide **1b** and the monosaccharide **1a**, but the latter has proven not to be an appropriate substrate for 1,3-1,4-β-glucanases as seen by the poor k_{cat}/K_M value for the wild-type enzyme (Table 2). Therefore, mutants at subsite −II are analyzed using eq 8 without subtracting any "background" effect, the meaning of $\Delta\Delta G^{\ddagger}_{mut-wt}$ being the overall effect of the mutation not directly assignable to individual protein−carbohydrate interactions. Table 7 summarizes the overall effect on TS

stabilization measured for the disaccharide **1b**, trisaccharide **1c** and tetrasaccharide **1d** substrates. Figure 6 illustrates the contacts in subsites −II and −I in the modeled E·S complex.

Glu61. Besides the interaction in subsite −III, Glu61 also hydrogen bonds with the 6-OH of Glc*p* −II as part of the bidentate H-bond. Mutation to Ala has an overall destabilizing effect of 6.5 kcal mol^{-1} with the trisaccharide substrate **1c**, which accounts for the disruption of both H-bond interactions. For the disaccharide substrate (**1b**) a loss of only 2.9 kcal mol^{-1} relative to the wt is measured, a value assignable to the interaction with the 6-OH Glc*p*-II. Then the contribution to TS stabilization of the H-bond between Glu61 and the 2-OH of Glc*p*-III is about 3.5 kcal mol^{-1}. Replacement to Gln(E61Q) changes a charged for an uncharged residue while maintaining the side chain length. The overall effect on trisaccharide kinetics is also a large destabilization of 5.2 kcal mol^{-1}. On the other hand, the E61D mutation results in a weaker effect, 4.1 kcal mol^{-1}. Therefore, the charge removal is more detrimental than shortening the side chain. For the disaccharide **1b**, both the Ala and Gln mutations give similar results, indicating that the Gln residue loses its H-bond capability in subsite −II. In addition, Glu61 mutants are the only ones to show regular Michaelis−Menten kinetics with the disaccharide **1b** (Table 3). In the wt, as well as in the rest of mutants analyzed, the bidentate H-bonding ability of Glu61 is unbalanced upon binding substrate **1b** (laminaribiosyl unit in subsites −II and −I). Whereas the H-bond with the 6-OH of Glc*p*-II may be maintained, the other carboxylate oxygen is left unligated and may be somehow responsible of driving the binding of a second molecule of substrate and give rise to the observed activation kinetics (Scheme 2). This activation behavior disappears upon removal of the glutamate side chain (E61A) or of the charged carboxylate (E61Q, where the H-bonding ability is largely eliminated as seen for the trisaccharide) and results in normal Michaelis−Menten kinetics for Glu61 mutants. This important role of Glu61 in subsite −III is consistent with the larger contribution of subsite −III to the overall transition-state stabilization in the wt enzyme according to the subsite mapping calculations.

Phe90. The phenyl ring is oriented perpendicular to the plane of the Glc*p* rings between subsites −II and −I (4.1 Å shortest carbon to carbon distance from the phenyl ring to Glc*p*−II and −I), and it may be involved in positioning the sugar substrate in the binding cleft and help create an hydrophobic environment. Mutation to Ala has a detrimental effect in catalysis with an overall destabilization of 4.7−4.9 kcal mol^{-1} with di-, tri-, and tetrasaccharide substrates.

Tyr92. Mutant Y92A was unstable under the standard conditions with substrates **1b**−**d**, precluding its kinetic characterization to evaluate the effect of removing the H-bond with 3-OH(Glc*p*−II) as well as the stacking interaction with the same Glc*p* ring. The aromatic side chain is close to the Trp101 and Tyr123 side chains, suggesting that they may interact and contribute significantly to keep the structural integrity of the protein fold. With laminarin as substrate (Table 1), a large reduction in k_{cat}/K_M is observed. The Y92W mutant has a detrimental effect on catalysis with an overall transition state destabilization of 1−1.5 kcal mol^{-1} depending on the substrate.

Asn180. Mutation to Ala introduces 5.4 kcal mol^{-1} overall destabilization with tri- and tetrasaccharide substrates, which includes the elimination of the H-bond between the amide function of Asn180 and the 6-OH of Glc*p*-II. Enlarging the side chain by mutation to Gln (N180Q) has approximately the same effect. This effect, too large for a single H-bond interaction, probably indicates an additional role of Asn180 in transition state stabilization.

Trp182. This tryptophan residue probably represents another system with an indirect effect on catalytic efficiency. The indol side chain is too far from the substrate molecule but it stacks with Phe28 [parallel aromatic rings at a distance of 4.08 Å in the free *B. macerans* enzyme (*12*)], which belongs to the major loop involved in substrate binding. The W182Y mutant produces 4.2 kcal mol^{-1} transition-state destabilization with the disaccharide substrate, and 3.5−3.7 kcal mol^{-1} with the tri- and tetrasaccharides. Mutation of the amino acid residue corresponding to Phe28 in the *B. licheniformis* 1,3-1,4-β-glucanase results in a similar energetic effect [3.6 kcal mol^{-1} TS destabilization with substrate **1c** (*20*)] in agreement with the coupling between both aromatic residues.

Subsite −I. In subsite −I, the protein−carbohydrate complex model is only tentative and preliminary since it does not take into account the expected glucopyranose ring distortion as argued in the Results. As for subsite −II mutants, the overall effect of the mutations is evaluated as $\Delta\Delta G^{\ddagger}_{mut-wt}$ with the same substrate (Table 7). Whereas the effect of the mutations on transition-state stabilization is obtained from k_{cat}/K_M values with substrates **1b**,**c**, the effect on ground-state binding is evaluated by means of inhibition kinetics with the competitive inhibitor **2** (Table 5). On the other hand, since the residues at this subsite are close to the catalytic machinery of the enzyme, the pH dependence of k_{cat}/K_M was determined for subsite −I mutants (Table 4).

Ser88. The side chain may form a hydrogen bond with the 6-OH group of Glc*p*-I. S88A shows an 8-fold reduction in k_{cat} and almost no change in K_M for di- and trisaccharide substrates, which corresponds to 1.0 kcal mol^{-1} TS destabilization, suggesting that the H-bond interaction may not be important in the ground state but stabilizes the transition state. However, from the inhibition constant of tetrasaccharide **2**, the contribution to ground-state binding accounts for 0.66 kcal mol^{-1} (weak H-bond, if it exists at all). The Ser to Ala mutation does not modify the kinetic pK_a values of the free enzyme (pH profile on k_{cat}/K_M).

Tyr121. The Y121F mutant has a slightly improved catalytic efficiency (in terms of k_{cat}/K_M) than the wt enzyme; removal of the tyrosine hydroxyl group results in 0.6 kcal mol^{-1} TS stabilization with both substrates **1b** and **1c**. It is mainly a K_M effect (3-fold decrease for substrate **1c**), but no change in the K_I value of the competitive inhibitor **2** is observed. Further mutation to Ala (Y121A) has important consequences: (a) 1.7 kcal mol^{-1} TS destabilization with the substrate **1c**, mainly arising from a k_{cat} reduction, (b) the K_I value for the inhibitor **2** is 10-fold lower than that of the wt enzyme, meaning 1.5 kcal mol^{-1} improved binding energy, and (c) the kinetic pK_a in the acidic limb (assignable to the catalytic nucleophile E105) is shifted upward 0.23 pH units relative to the wt enzyme, whereas the Y121F mutant has essentially the wild-type kinetic pK_a values. Altogether, these results indicate that the tyrosine hydroxyl group is not important for activity and also does not contribute to ligand

binding in subsite −I, but the aromatic ring seems to be relevant. Interactions at the 2-hydroxyl position of the saccharide are important for transition-state stabilization in a number of glycosidases, providing up to 10 kcal mol^{-1} stabilization (*34*, *35*), but the identity of the amino acid residues involved is not clearly established. In the case of the β-1,4-glycosidase Cex from *Cellulomonas fimi* (*36*), where the 3D-structure of the covalent glycosyl−enzyme intermediate using an inactive mutant form has been visualized by X-ray crystallography, the side-chain carbonyl oxygen of the catalytic nucleophile has been proposed to play this role. The 2-hydroxyl position of the sugar has a close, low-barrier type (*37*, *38*), H-bond interaction with the carboxylate of the nucleophile residue, and other possible interactions with surrounding residues may not be major contributors to TS stabilization. Since this interaction may become optimized geometrically and electronically as the transition state is reached (*36*), the proposed Glu-C=O··· HO-2 interaction may prove to be a widespread mechanism of TS stabilization in β-glucosyl hydrolyzing enzymes.

From the results reported here, Tyr121 does not play a role in TS stabilization through hydrogen bonding. But the aromatic tyrosine ring has an effect both on ground-state binding and on transition-state stabilization. Tyr121 has a favorable stacking interaction with Trp101 in the free enzyme, which in turn hydrogen bonds to the catalytic nucleophile. If this interaction network is important to position the nucleophile side chain, the Y121A mutation may have an indirect effect disturbing the H-bond Trp101··· Glu103. Consistent with this, the pK_a of the nucleophile Glu103 is slightly rised, the catalytic efficiency is decreased, and tighter binding of inhibitor **2** can arise from an improved H-bond between the 2-OH(Glc*p*-I) and the nucleophile residue due to the different orientation of the carboxyl side chain, suboptimal for transition-state stabilization but maybe able to interact in the ground state. This tentative interpretation requires additional structural support, i.e., from an X-ray structure of a noncovalent enzyme−inhibitor complex when available.

Lichenan Kinetics. As a polysaccharide substrate, lichenan fills the entire binding cleft of the enzyme in the productive complex. The effects of the mutations in subsites −IV to −I measured as $\Delta\Delta G^{\ddagger}_{mut-wt}$ (Table 1) are consistent with the above analyses using the 4-methylumbelliferyl oligosaccharides. A good correlation of $\Delta\Delta G^{\ddagger}_{mut-wt}$ values (Figure 7) between lichenan and the tetrasaccharide **1d** (for mutants at subsites −IV, −III, and −II) or the trisaccharide **1c** (for subsite −I mutants) is observed, but the magnitudes are slightly lower for lichenan in all cases. Two mutations, Y22W and Y121F, produce enzyme variants with improved catalytic efficiency as the result of lower K_M values.

Subsite +I. Asn119, Glu129, and Trp190 may interact with the substrate according to the modeled E·S structure (Figure 6). The mutants at these residues have been only characterized with the chromophoric substrate **1c**, which places a methylumbelliferyl group in subsite +I, the effect being less than 0.9 kcal mol^{-1} TS destabilization in all cases (Table 7). Careful analysis of subsite +I mutants is out of the scope of the present work since other substrates with a glucopyranose unit instead of an aromatic aglycon in subsite +I will be required. Preliminary results are obtained from the

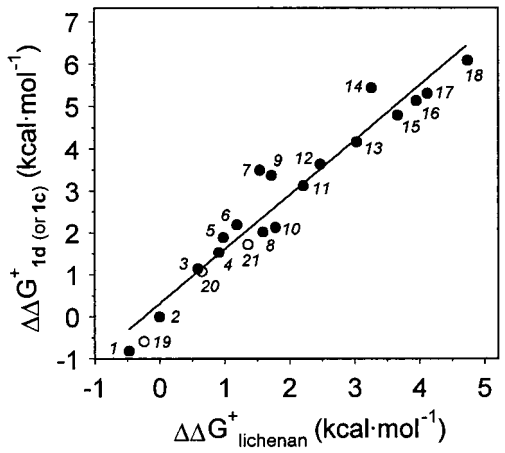

FIGURE 7: Correlation of $\Delta\Delta G^{\ddagger}_{wt-mut}$ values between lichenan and substrate **1d** for mutants at subsites −IV to −II (●), and between lichenan and substrate **1c** for subsite −I mutants (○). Mutants: (1) Y22W, (2) H143A, (3) H97D, (4) Y92W, (5) R63K, (6) R63A, (7) W182Y, (8) Y22F, (9) N24Q, (10) H97R, (11) Y22A, (12) N24A, (13) E61D, (14) N180Q, (15) F90A, (16) E61Q, (17) N180A, (18) E61A, (19) Y121F, (20) S88A, (21) Y121A.

kinetics with lichenan (Table 1). Mutants N119D,L, E129Q, and W190A all show reduced catalytic efficiency in terms of k_{cat}/K_M, with $\Delta\Delta G^{\ddagger}$ values ranging 2−4.4 kcal mol^{-1}. These values are larger than those found with substrate **1c** because a glucose unit of lichenan in subsite +I will establish a number of interactions which are expected to be weaker or missing with the 4-methylumbellyferyl aglycon. Work is in progress for such a detailed analysis.

Sequence Comparison. The residues analyzed in this work have been proposed as being involved in substrate binding on the basis of the modeled enzyme−substrate complex structure. Amino acid sequence comparison to related enzymes (Figure 8) provides additional information about changes tolerated in some of the residues, and their effect on substrate specificity. Glu61, Ser88, Phe90, Tyr92, Glu107, Asn119, Glu129, Asn180, Trp182, and Trp190 are strictly conserved in bacterial 1,3-1,4-β-glucanases (lichenases, EC 3.2.1.73) as shown in Figure 8. The same residues are invariant in ExoK from *Rhizobium melilotii* (sp P333693) except Ser88 (replaced by Ala) and Asn180 (replaced by Ser). The enzyme might be involved in the cleavage of high molecular weight succinoglycan into the low molecular weight form (*39*) and displays 1,3-1,4-β-glucanase activity (Piotukh, unpublished results). The plant xyloglucan endo transglycosylases, XET (EC 2.4.1.207), able to catalyze both endo-type splitting of a xyloglucan molecule, and linking of a newly generated reducing end to the nonreducing end of another xyloglucan molecule (*40*) are related in their primary sequences to bacterial lichenases (*41*), and the residues Glu107, Asn119, Glu129, Trp182, and Trp190 remain invariant. However, E61 and the other residues involved in substrate binding at subsites −III and −II are not conserved pointing to altered substrate specificity. The change Y22W is tolerated in various lichenases, and Tyr121 is replaced by Phe in alkalophilic glucanases and might be the cause of increased activity toward laminarin.

Substrate Specificity. Why does the enzyme require a β-1,3 linkage between subsites −I and −II and a β-1,4 linkage between subsites −II and −III? In the modeled E·S complex, the oligosaccharide chain describes an extended path with

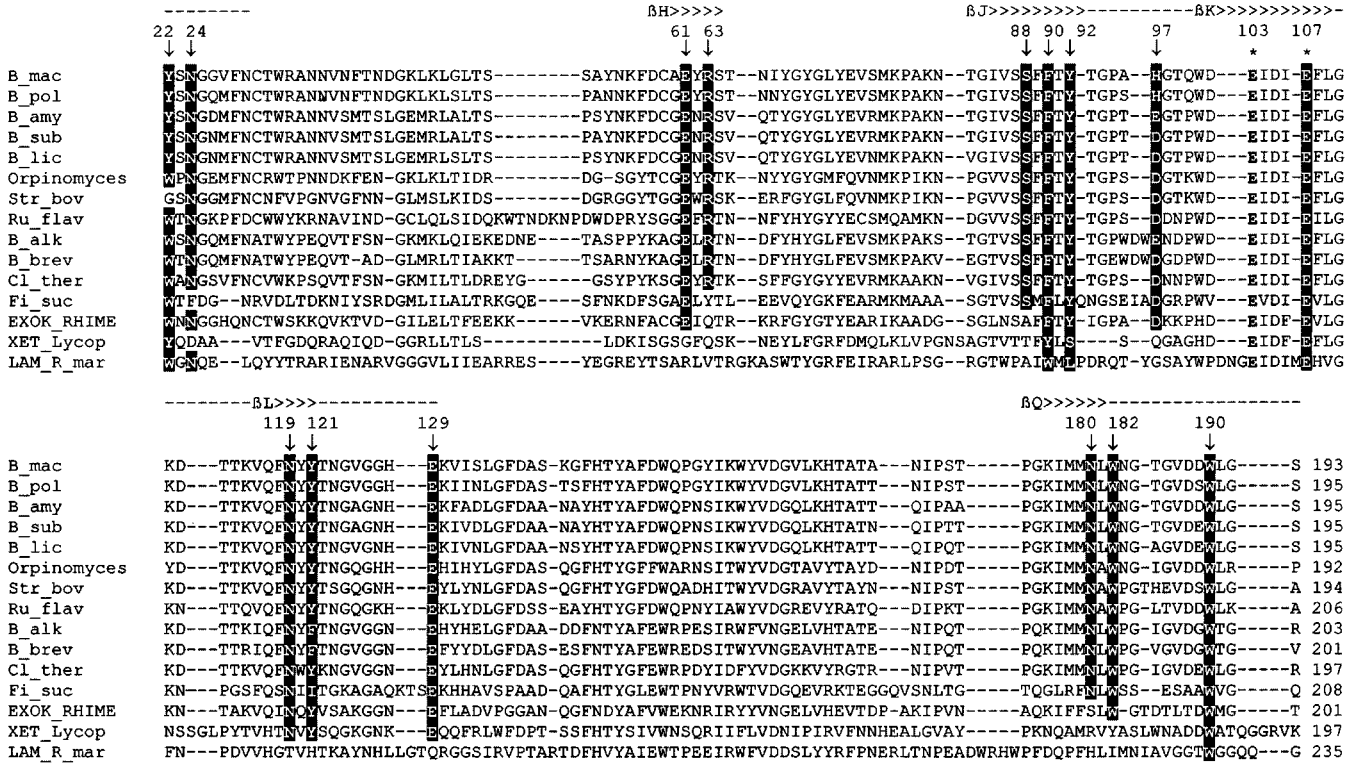

FIGURE 8: Sequence comparison of mature *B. macerans* β-glucanase with other microbial lichenases and related enzymes belonging to glycosyl hydrolase family 16. Vertical arrows delineate residues replaced in *B. macerans* 1,3-1,4-β-glucanase mutants. Residues invariant in all lichenases are underlined. Asterisks label the active-site residues E103 and E107. Abbreviations and accession numbers: (lichenases): B_mac, *B. macerans* spP23904; B_pol, *Paenibacillus polymyxa* spP45796; B_amy, *B. amyloliquefaciens* gbM15674; B_sub, *B. subtilis* trU60830; B_lic *B. licheniformis* Z29515; Orpinomyces, *Orpinomyces sp.* PC-2 U63813; Str_bov, *Streptococcus bovis* Z92911; Ru_flav, *Ruminococcus flavefaciens* S61204; B_alk, alkalophilic *Bacillus* strain N137 Z12151; B_brev, *B. brevis* M84339; Cl_ther, *Clostridium thermocellum* X63355; Fi_suc, *Fibrobacter succinogenes* strain S85 M33676; (other activities): ExoK_RHIME, ExoF from *Rhizobium melilotii* Z17219; XET_Lycop, XET from *Lycopersicon esculentum* X82684; Lam_R_mar, laminarinase *from Rhodotermus marinus* AF47003. (- - -) loop region, β >>>>, β-sheet according to the nomenclature given in ref *21*.

the tetrasaccharide part in subsites −I to −IV having a conformation close to that of the free molecule in solution [as studied by NMR spectroscopy (*42*)]: two glucopyranose units linked by a β-1,3 bond have the Glc*p* rings in the same orientation, i.e., the 6-CH_2OH side chains pointing to the same face, whereas a β-1,4 linkage renders both Glc*p* in alternating conformations, the 6-CH_2OH side chains at approximately 180°. When the Glc*p* ring in subsite −I is properly oriented for catalysis, the Glc*p* in subsite −II has the same orientation, as corresponds to a β-1,3 linkage. For subsite −III, the required β-1,4 bond positions the Glc*p* ring in the alternate orientation, while subsite −IV can accommodate both [Glc*p*-β(1→4) in barley β-glucan, and Glc*p*-β(1→3) in the reduced pneumococcal polysaccharide, a glucan with alternating β-1,3 and β-1,4 glycosidic bonds (*1*)]. When comparing the relative ring orientations with those of laminarin and cellulose derivatives, which are not substrates, the major differences are in subsites −II and −III. The reported mutational analysis shows that the glucopyranose rings at these subsites are tightly bound by a number of hydrogen bond interactions involving most of the hydroxyl groups of the sugar. Glu61, Asn24, Tyr92, and Asn180 establish a hydrogen bond network with the substrate, thus positioning the cellobiosyl unit in a specific orientation in subsites −III and −II. By contrast, the single stacking interaction between Tyr22 and the Glc*p*-IV ring may allow binding of both orientations in subsite −IV.

The mutational analysis reported here provides important functional information of the role of amino acid residues in the binding cleft and the magnitude of the protein−substrate interactions. Structural data from X-ray crystallography of an E·S complex (with an inactive mutant) will complete the detailed description of the specificity of *Bacillus* 1,3-1,4-β-glucanases.

ACKNOWLEDGMENT

We thank Dr. Udo Heinemann for providing the PDB file of the modeled enzyme−substrate complex structure reported in Hahn et al. (1995) (ref *22*).

REFERENCES

1. Anderson, M. A., and Stone, B. A. (1975) *FEBS Lett. 52*, 202−207.
2. Stone, B. A., and Clarke, A. E. (1992) *Chemistry and Biology of (1→3)-β-glucans*, La Trobe University Press, Bundoora, Australia.
3. Henrissat, B. (1991) *Biochem. J. 280*, 309−316.
4. Henrissat, B., and Bairoch, A. (1996) *Biochem. J. 316*, 695−696.
5. Borriss, R. (1994) *Curr. Top. Mol. Genet. 2*, 163−188.
6. Ekinci, M. S., McCrae, S. I., and Flint, H. J. (1997) *Appl. Environ. Microbiol. 63*, 3752−3756.
7. Chen, H. Li, X.-L., and Ljungdahl, L. G. (1997*) J. Bacteriol. 179*, 6028−6034.
8. Malet, C., Jiménez-Barbero, J., Bernabé, M., Brosa, C., and Planas, A. (1993) *Biochem. J. 296*, 753−758.
9. Sinnott, M. L. (1990) *Chem. Rev. 90*, 1171−1202.

10. Davis, G., Sinnott, M. L., and Withers, S. G. (1997) in *Comprehensive Biological Catalysis* (Sinnott, M. L., Ed.) pp 119−209, Academic Press, London.
11. Juncosa, M., Pons, J., Dot, T., Querol, E., and Planas, A. (1994) *J. Biol. Chem. 269*, 14530−14535.
12. Hahn, M., Olsen, O., Politz, O., Borriss, R., and Heinemann, U. (1995) *J. Biol. Chem. 270*, 3081−3088.
13. Viladot, J. LL., de Ramón, E., Durany, O., and Planas, A. (1998) *Biochemistry 37*, 11332−11342.
14. Malet, C., Viladot, J. L., Ochoa, A., Gállego, B., Brosa, C., and Planas, A. (1995) *Carbohydr. Res. 274*, 285−301.
15. Malet, C., Vallés, J., Bou, J., and Planas, A. (1996) *J. Biotechnol. 48*, 209−219.
16. Malet, C., and Planas, A. (1997) *Biochemistry 36*, 13838−13848.
17. Planas, A., Millet, O., Palasí, J., Pallarés, C., Abel. M, and Viladot, J. L. (1998) *Carbohydr. Res. 310*, 53−64.
18. Hahn, M., Pons, J., Planas, A., Querol, E., and Heinemann, U. (1995) *FEBS Lett. 374*, 221−224.
19. Heinemann, U., Aÿ, J., Gaiser, O., Müller, J. J., and Ponnuswamy, M. N. (1996) *Biol. Chem. 377*, 447−454.
20. Pons, J., Querol, E., and Planas, A. (1997) *J. Biol. Chem. 272*, 13006−13012.
21. Keitel, T., Simon, O., Borriss, R., and Heinemann, U. (1993) *Proc. Natl. Acad. Sci. U.S.A. 90*, 5287−5291.
22. Hahn, M., Keitel, T., and Heinemann, U. (1995) *Eur. J. Biochem. 232*, 849−859.
23. Borriss, R., Buettner, K., and Maentsaelae, P. (1990) *Mol. Gen. Genet. 222*, 278−283.
24. Landt, O., Grunert, H. P., and Hahn, U. (1990) *Gene 96*, 125−128.
25. Teather, R. M., and Wood, P. J. (1982) *Appl. Environ. Microbiol. 43*, 777−780.
26. Politz, O., Simon, O., Olsen, O., and Borriss, R. (1993) *Eur. J. Biochem. 216*, 829−34.
27. Hahn, M., Piotukh, K., Borriss, R., and Heinemann, U. (1994) *Proc. Natl. Acad. Sci. U.S.A. 91*, 10417−10421.
28. Laemmly, U.K. (1970) *Nature 227*, 680−685.
29. Bradford, M. M. (1976) *Anal. Biochem. 72*, 248−254.
30. Hinchliffe, E. (1984) *J. Gen. Microbiol. 130*, 1285−1291.
31. van Tilbeurgh, H., Claeyssens, M., and de Bruyne, C. K. (1982) *FEBS Lett. 149*, 152−156.
32. Sulzenbacher, G., Driguez, H., Henrissat, B., Schülein, M., and Davies, G. J. (1996) *Biochemistry 35*, 15280−15287.
33. Davies, G. J., Mackenzie, L. Varrot, A., Dauter, M., Brzozowski, A. M., Schülein, M., and Withers, S. G. (1998) *Biochemistry 37*, 11707−11713.
34. Namchuk, N. M., and Withers, S. G. (1995) *Biochemistry 34*, 16194−16202.
35. McCarter, J. D., Adam, M. J., and Withers, S. G. (1992) *Biochem. J. 286*, 721−727.
36. Notenboom, V., Birsan, C., Nitz, M., Rose, D. R., Warren, R. A. J., and Withers, S. G. (1998) *Nat. Struct. Biol. 5*, 812−818.
37. Guthrie, J. P. (1996) *Chem. Biol. 3*, 163−170.
38. Gerlt, J. A., Kreevoy, M. M., Cleland, W. W., and Frey, P. A. (1997) *Chem. Biol. 4*, 259−267.
39. Becker, A., Kleickmann, A., Arnold, W., and Puehler, A. (1993) *Mol. Gen. Genet. 238*, 145−154.
40. Nishitani, K., and Tominaga R. (1992) *J. Biol. Chem. 267*, 21058−21064.
41. Okazawa, K., Sato, Y., Nakagawa, T., Asada, K., Kato, I., Tomita, E., and Nishitani, K. (1993) *J. Biol. Chem. 268*, 25364−25368.
42. Bernabé, M., Jiménez-Barbero, J., and A. Planas (1994) *J. Carbohydr. Chem. 13*, 799−817.
43. Kraulis, J. P. (1991) *J. Appl. Crystallogr. 24*, 946−950.

BI991690Q